PNAS

Supporting Information for

Molecularly confined hydration in thermoresponsive hydrogels for efficient atmospheric water harvesting

Weixin Guan[1], Yaxuan Zhao[1], Chuxin Lei, and Guihua Yu*

Materials Science and Engineering Program and Walker Department of Mechanical Engineering, The University of Texas at Austin, Austin, TX 78712, USA

*E-mail: ghyu@austin.utexas.edu

Table of Contents

S1.1 Solar-driven desorption setup

To measure the kinetics of solar-driven water release, the petri dish loaded with samples surrounded by thermal insulation substrate is placed on a microbalance with the data acquisition system. The simulated solar light source is placed above the microbalance. The light intensity is adjusted by changing the sample height.

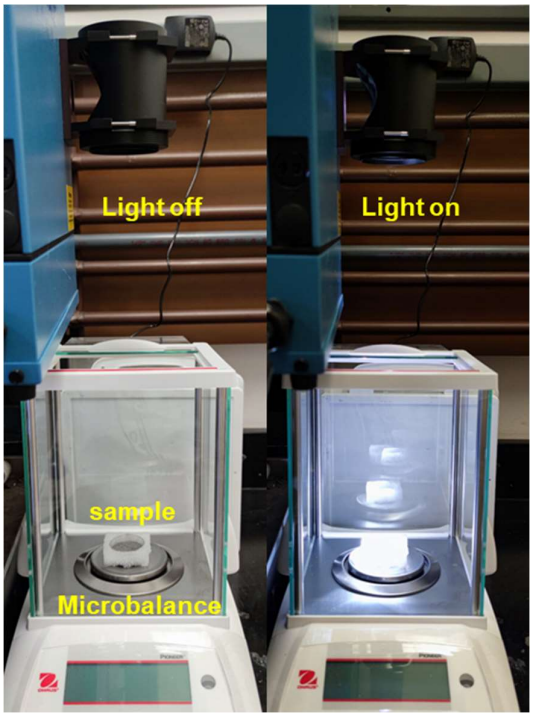

Figure S1. **Solar-driven desorption setup**. Schematic of the homemade solar-driven water release system.

S1.2 Water vapor sorption measurement

The homemade water vapor sorption system consists of three parts: a moisture generator, a testing chamber, and a hygrometer (Figure S2). Supersaturated salt solutions are used to generate moisture flow with controlled RH by supplying dehydrated nitrogen flow into solutions. Typically, supersaturated CH_3CO_2K and NaBr solutions are used for ca. 30% and 60% RH conditions, with a 250 mL/min flow rate (1). The testing chamber is sealed by a rubber ring and placed on a microbalance. The hygrometer is inserted to monitor the RH and temperature in the sorption chamber. Before the water vapor sorption measurement, all samples are dried in a vacuum oven at 90 °C for at least 2 h. The weight change was obtained by microbalance.

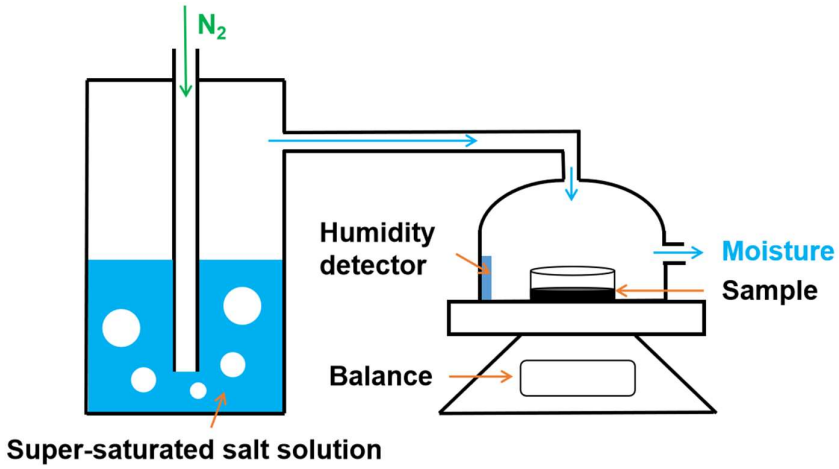

Figure S2. **Water vapor sorption measurement setup**. Schematic of the homemade water vapor sorption system.

S2.1 Schematic of phase transition of PNIPAM

Poly(N-isopropylacrylamide) (PNIPAM) is a thermoresponsive polymer, characterized by a lower critical solution temperature (LCST) phenomenon, which typically occurs around 32°C. Above this threshold, the polymer undergoes a coil-to-globule conformational transition due to alterations in the balance of hydrophilic and hydrophobic interactions.

In aqueous environments below the LCST, PNIPAM exhibits solubility as a result of favorable interactions between amide moieties within the polymer backbone and water molecules. These amide groups participate in hydrogen bonding with water, enhancing the polymer's hydrophilic character. Meanwhile, isopropyl side chains are solvated by water molecules, although no hydrogen bonding occurs, in a process referred to as hydration. Upon elevating the temperature, the hydrophobic associations among isopropyl side chains become more pronounced. Consequently, water molecules proximal to these side chains are displaced, resulting in the dehydration of methyl groups. Simultaneously, the hydrogen bonding between amide groups and water molecules weakens due to disruptions in the water structure surrounding the polymer chains and an increase in system entropy. This scenario also promotes long-range interactions between intra-polymer chains. The net effect of these conformational changes is a reduction in the polymer's solubility. Collectively, these molecular-scale phenomena drive the collapse and aggregation of the polymer chains, culminating in the observed phase transition (2, 3). This conformational change in PNIPAM can be harnessed for AWH applications, where the sorbent's temperature-sensitive behaviour facilitates the desorption process. As the temperature rises above the LCST, the hydrophobic collapse of the

polymer promotes water release from the sorbent, enabling efficient water recovery and regeneration of the material for subsequent cycles of water capture and release.

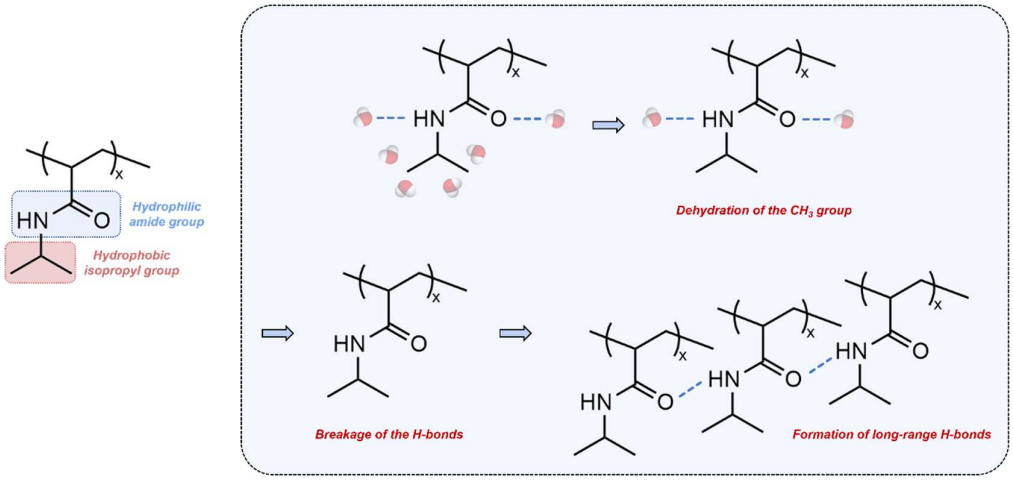

Figure S3. **Mechanism of conformational change in PNIPAM at LCST.** The hydrophobic interaction of the methyl group and hydrogen bonding breakage induce the phase transition.

S2.2 Comparison of salt and hydrogel-mediated sorbents for AWH

A qualitative comparison of different materials for AWH is provided in terms of water uptake, kinetics, desorption efficiency and cyclability (Fig. 1c and Table 1). Desorption is a key process for sorbents to release the absorbed water by heating. Sorbents with high desorption efficiency can release most of water under relatively low temperature, which can largely reduce the energy consumption for water production. In this case, we use the reported lowest temperature that can realize the desorption of 80% water uptake to represent the desorption efficiency of the sorbent. Hygroscopic salts show high vapor sorption capacity (4), but they are easy to deliquesce (5), which will result in sluggish kinetics due to the passivation layer formation. Salt-based hydrogels generally refer to a class of materials with hydroscopic salt embedded into a polymer matrix. Although the kinetics can be improved by storing the salt solution within the gel network (6, 7), salt confinement is still not sufficient that aggregated salt hydrates will still be formed during water sorption process. Since hydrates have high activation energy of decomposition, high desorption temperature is required to release that part of water, and thus results in lowered desorption efficiency (8, 9). Besides, polymers suffering from salting-out effect, like PNIPAM, typically have poor swelling ability (10, 11), which may risk salt leakage under high RH, resulting in deteriorated cyclability (12). Our confined hydration hydrogel is composed of zwitterionic moieties (PDMAPS) and thermoresponsive moieties (PNIPAM). The strong immobilization of salt ions within PDMAPS will help construct a confined water network without the formation of salt hydrates, while the conformational change within PNIPAM will also facilitate water release during desorption. Their synergistic contributions endow our system with high desorption efficiency. In addition,

the diffusion length will be largely shortened by the microgel configuration, which will further enhance the kinetics of our system (13).

Supplementary Table 1. Evaluation matrices of the cross-comparisons in terms of water uptake, kinetics and desorption efficiency.

Score	Water uptake at 60% RH (g g^{-1})
1	<0.6
2	0.6-0.8
3	0.8-1.0
4	1.0-1.2
5	>1.2
Score	Time to reach 80% water uptake at 60% RH (min)
1	>200
2	150-200
3	100-150
4	50-100
5	<50
Score	Reported lowest temperature to desorb 80% water uptake (℃)
1	>95
2	95-80
3	80-65
4	65-50
5	<50

S2.3 Optimizing the concentration of salt solution for ion loading

The saturated water content of hydrogel (Q, g g^{-1}) swelling in the salt solution with different concentrations is calculated by the following equation,

$$Q = \frac{m_t - m_0}{m_0}$$

where m_t and m_0 are the weights of the hydrogels in the dry state and swollen state at a certain time, respectively. From Figure S4, we can find that PDMAPS only absorbs ~3 g g^{-1} liquid in pure water, while this value boosts to ~12 g g^{-1} in 4M LiCl solution. This enhanced swellability of PDMAPS hydrogel confirms that the salt solution can break the self-association between the $-N^+(CH_3)^{2-}$ and $-SO_3^-$ caused by the electrostatic interactions. Although the swelling ratio steadily decreased as the concentration of LiCl solution increased over 4M, it remained greater than that of pure water. In the presence of LiCl salt, the resulting nonassociated hydrogels have dramatically increased swelling capacity, potentially allowing for more productive water vapor sorption (10, 11, 14).

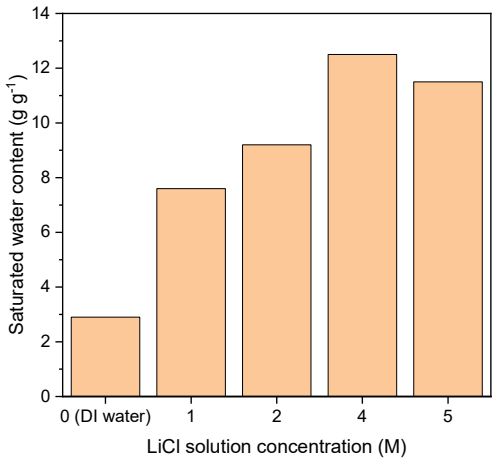

Figure S4. **Optimizing the concentration of salt solution for ion loading**. The values of the saturated water content of PDMAPS hydrogel swelling in DI water and LiCl solution with different concentrations.

S2.4 Ion content in TZMGs

Figure S5 shows the results of the TG analysis. The polymer begins to decompose at around 280 ºC ensuring the stability of hydrogels in the desorption process. Polymer networks can completely decompose and escape under the high temperature of 600 °C, while the remaining weight is the mass of ion species. The loaded salt ion weight ranges from 17.82 wt% of TZMG-1.0 to 6.68 wt% of TZMG-0.1.

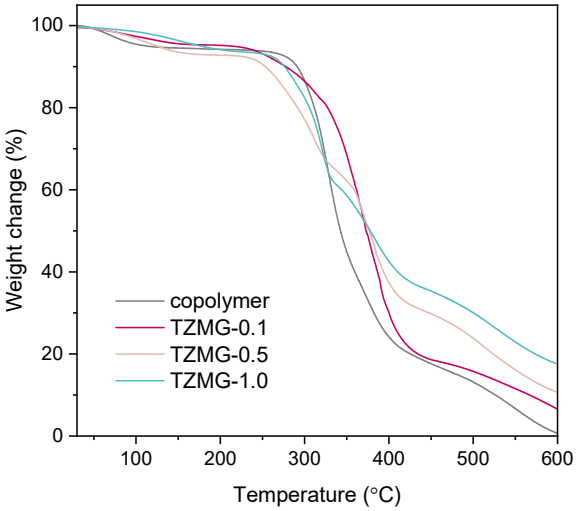

Figure S5. **Ions content in TZMGs**. TGA curves of TZMGs.

S2.5 Morphology characterization of TZMGs

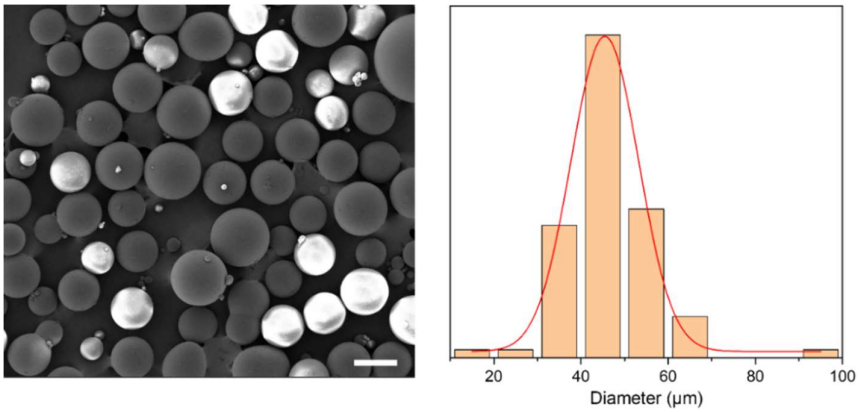

Figure S6. **SEM images and diameter distribution of TZMGs**. Scale bar: 50 μm.

S2.6 Water vapour sorption-desorption performance of TZMGs

Figure S7a show the static vapour sorption-desorption performance of TZMGs, in which TZMG-0.1 to 1.0 show increased water uptake with similar kinetics. Figure S7b shows the weight change rate in the sorption and desorption process of TZMGs. It can be found that the sorption reaches equilibrium within 100 min featured by weight change rate ≈ 0 g g^{-1} min^{-1}.

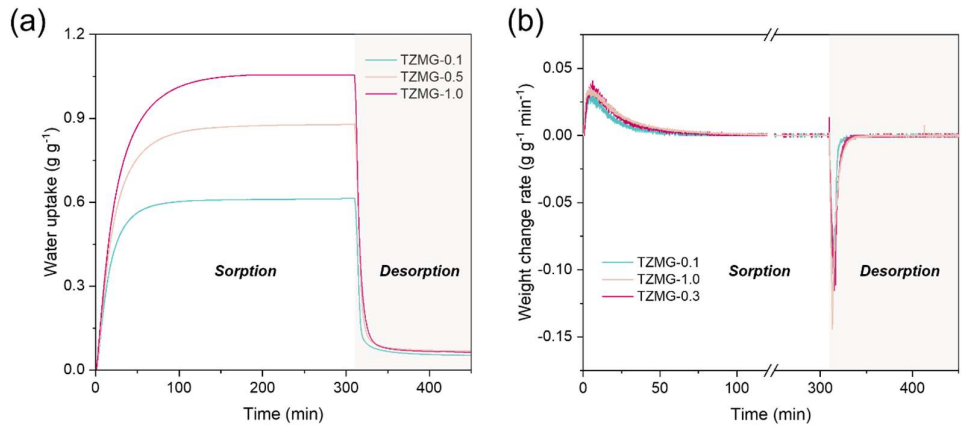

Figure S7. **Sorption and desorption rate of TZMGs**. Sorption conditions: 60% RH, 25 °C. Desorption conditions: 60 °C and water vapor pressure of 3.17 kPa.

S2.7 Temperature-dependent desorption behaviour of TZMG-1.0

Figure S8 shows the desorption curve in a static DVS test with the sorption condition of 30% RH and varying desorption temperatures. The captured water in TZMG-1.0 can be released by approximately 80% within 10 minutes through mild heating at 60°C. Furthermore, TZMG-1.0 can discharge over 80% of absorbed water within around 25 minutes at a relatively low temperature of 40°C.

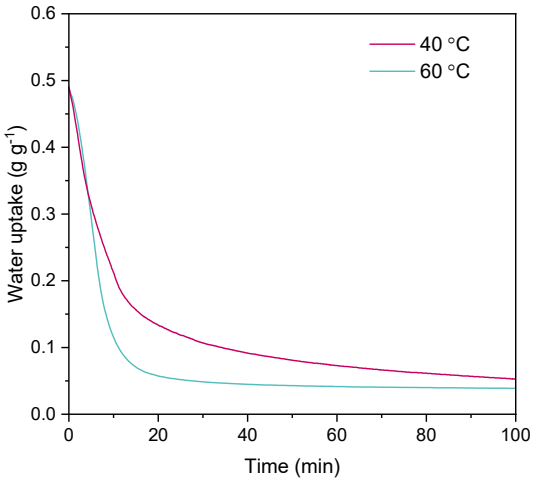

Figure S8. **Temperature-dependent desorption behaviour of TZMG-1.0**. Sorption conditions: 30% RH, 25 °C. Desorption conditions: 60 °C and water vapor pressure of 3.17 kPa.

S2.8 Static sorption-desorption properties of PNIPAM-LiCl

Figure S9 shows the sorption-desorption properties of PNIPAM-LiCl in a static DVS test with the sorption condition of 60% RH and varying desorption temperatures. The PNIPAM-LiCl sample was chosen with similar water uptake at 60% RH to compare the desorption behaviour. Due to the slow kinetics of salt deliquescence and the reduced hydrability of PNIPAM in response to salt ions, the PNIPAM-LiCl hydrogel cannot reach equilibrium within 6 h. Moreover, salt-dominating moisture harvesting inhibits the complete release of captured water. It cannot reach 80% release of captured water at 40 °C within 120 min. Also, it takes more than an hour to achieve 80% release of captured water at 60 °C. Such a desorption behaviour proves that the proposed confined hydration design has the advantages of energy-efficient water release.

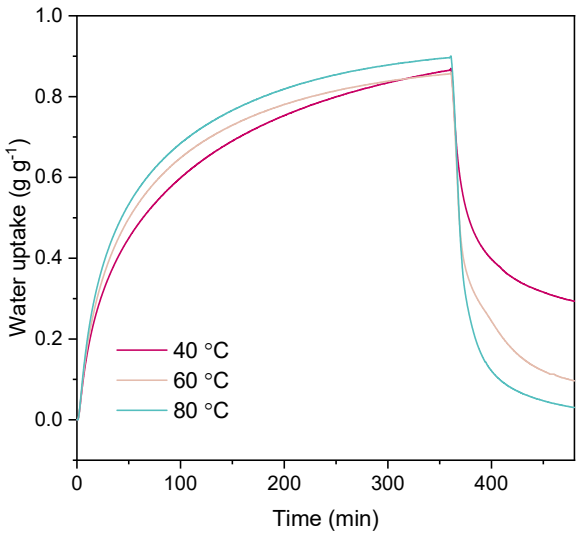

Figure S9. **Static sorption-desorption properties of PNIPAM-LiCl**. Sorption conditions: 60% RH, 25 °C. Desorption conditions: 60 °C and water vapor pressure of 3.17 kPa.

S2.9 Evaporation profiles of PNIPAM-LiCl, PDMAPS-LiCl, and pure LiCl

Figure S10a presents the evaporation peaks of LiCl at ~46, 70, and 95 °C. Respectively, these correspond to three distinct stages of the desorption process: 1) evaporation from bulk solution at ~46 °C, 2) crystallization of LiCl at ~70 °C - an endothermic process transitioning from a hydrated, disordered state to a more ordered crystalline state, and 3) chemical desorption of LiCl at ~95°C, where chemisorbed water molecules are released (9). These stages collectively represent the complex desorption behavior of LiCl. For the hydrogel/LiCl composites, PNIPAM-LiCl first presents a major evaporation peak at 32 °C, consistent with the reported lowest critical solution temperature (LCST) of PNIPAM (Figure S10b) (15). The second evaporation peak at ~70 °C should be assigned to the dehydration of LiCl crystalline (8). The subtle final peak can be attributed to the chemical desorption of LiCl embedded within the PNIPAM matrix. The peak's weak intensity is a result of two primary factors: 1. The salt content is relatively low, at approximately 7.5 wt% as per the TGA results shown in Figure S11. The strong salting-out effect restricts the PNIPAM network's swelling capacity, leading to low salt loading. 2. The water chemisorbed by LiCl constitutes the smallest portion of the total water uptake in the PNIPAM-LiCl hydrogels. The majority of water is associated with the polymer network, with a smaller portion strongly interacting with salt ions. During the desorption process, the latter mostly appears as salt hydrate, leaving a small fraction as chemisorbed water. As a comparison, PDMAPS-LiCl only exhibits a main evaporation peak at 56 °C without any secondary peak, implying that the hygroscopicity of zwitterionic hydrogel originates from the confined ion-pairs instead of the hydrated salt crystalline. By further

incorporating the thermoresponsive NIPAM segment, the evaporation temperature can be lowered to below 40 °C as shown in the main text (Figure 3D).

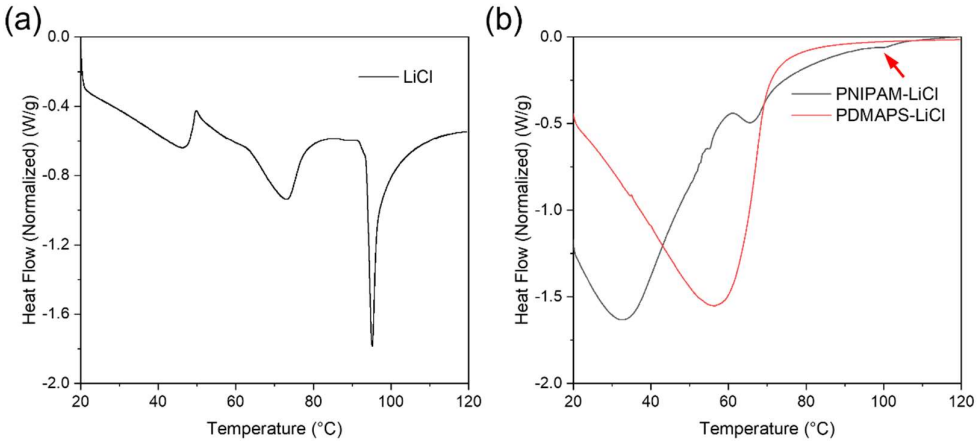

Figure S10. **Evaporation behaviors of hydrogels and salt**. DSC profiles of (a) pure LiCl, and (b) PNIPAM-LiCl and PDMAPS-LiCl. All samples are hydrated with water uptake of 1 g g^{-1}.

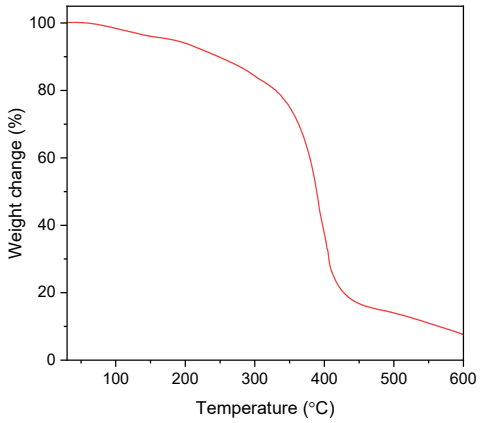

Figure S11. **Salt content in PNIPAM-LiCl**. TGA curves of PNIPAM-LiCl hydrogel.

S2.10 Desorption properties of TZMGs

In our analysis of the thermoresponsive desorption behavior of TZMGs, we took into account the fundamental interplay between the hydrogel's hydrophilicity-hydrophobicity transition and the associated water release mechanism. Our investigation focused on copolymer hydrogels with varying ratios of NIPAM:DMAPS.

The augmented incorporation of hygroscopic zwitterionic DMAPS segments enhances the hydrophilicity of the hydrogels. This not only elevates the phase transition temperature but also diminishes the degree of the phase transition. This behavior could potentially counteract the gel's water release capability due to a reduction in overall temperature-induced hydrophobicity. Nonetheless, the hydrophilic-hydrophobic switching behavior of the NIPAM moieties remains functional even with the introduction of additional zwitterionic units. These switches lead to changes in the network conformation, disrupting the hydrogen-bonding water network and facilitating the desorption process.

We conducted desorption tests at 40°C on three copolymer hydrogels: TZMG-0.1, TZMG-0.5, and TZMG-1.0. The results, as shown in Figure S12, indicated a decreasing trend in the desorption degree with increased DMAPS content. This observation can be accounted for by two interconnected factors. Firstly, the phase transition temperature ascends with a greater inclusion of zwitterionic DMAPS segments. As such, at 40°C, the hydrogel with a higher DMAPS ratio (TZMG-1.0) exhibits superior water-repelling capabilities compared to a hydrogel with a lower DMAPS ratio (TZMG-0.1), where the hydrophobicity transition is just initiating. Secondly, in the case of TZMG-1.0, a considerable portion of water molecules is

engaged in interactions with the zwitterions. This interaction necessitates a higher activation energy for desorption, contributing to a reduced degree of water release at 40 °C.

These findings, in harmony with our observations in Figure 3D, elucidate the nuanced influence of the DMAPS ratio on the thermoresponsive desorption behavior of our TZMGs. Consequently, this highlights the necessity of optimizing the NIPAM:DMAPS ratio to tailor the desorption properties of the hydrogel for specific applications.

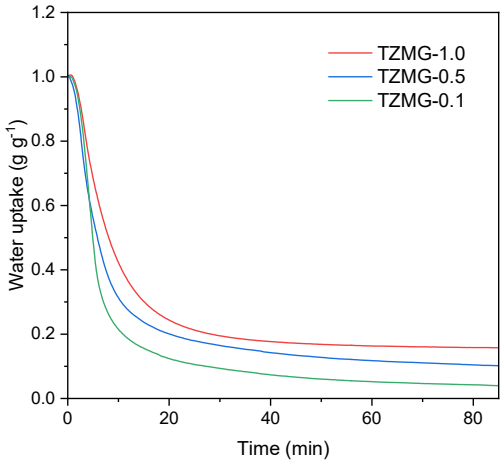

Figure S12. **Desorption curves of TZMGs.** The desorption is conducted at 40 °C and a water vapor pressure of 3.17 kPa.

S2.11 AWH performances comparison with reported salt-contained gel-based sorbents

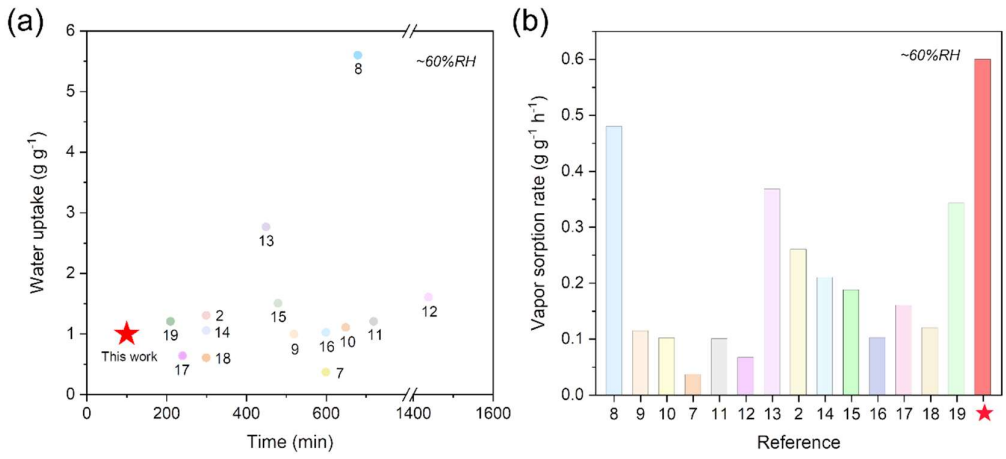

Figure S13. **AWH performance comparison.** (a) Scattering plot of water uptake at 60% RH vs. time to reach equilibrium.(b) Corresponding vapor sorption rate plot. (6, 7, 11, 12, 16-24)

S2.12 Comparison of desorption performance with start-of-the-art salt-contained gel-based sorbents.

Supplementary Table 2. Detailed desorption properties of sorbents with ~30% RH sorption.

Materials	Sorption RH (%)	Desorption Temperature (°C)	Desorption Time (min)	Desorbed Water (g/g)	Ref.
Ca^{2+}/Li^{+}@alginate+CNT	20	80	155	1.138	(12)
PAM+$CaCl_2$+CNT	35	85	41	0.382	(7)
Biochar+SA+$CaCl_2$	20	80	22	0.425	(6)
LiCl@rGO-SA	30	90	85	1.218	(18)
		80/70/60	Can't desorb 80% wu		
Alginate@melamine foam+$CaCl_2$	20	80	25	0.48	(19)
Carbon sphere+LiCl	35	80	32	0.557	(25)
Alginate-$CaCl_2$	25	100	303	0.481	(26)
HPC+LiCl	30	60	15	0.648	(27)
		50	Can't desorb 80% wu		
KGM+HPC+LiCl	30	60	15	0.745	(28)
PAM+LiCl	20	60	53	0.855	(8)
PDMAPS+LiCl	30	80	78	0.495	(10)
PNIPAM-co-DMAPS+	30	**60**	10	0.384	This work
LiCl	30	**40**	27	0.384	

Supplementary Table 3. Detailed desorption properties of sorbents with ~60% RH sorption.

Materials	Sorption RH (%)	Desorption Temperature (°C)	Desorption Time (min)	Desorbed Water (g/g)	Ref.
Ca^{2+}/Li^{+}@alginate+CNT	70	80	23	4.492	(12)
PAM+$CaCl_2$+CNT	60	85	36	0.806	(7)
PAETA-Cl	60	70	31	0.237	(29)
PAETA-Ac	60	70	27	0.36	
Biochar+SA+$CaCl_2$	50	80	20	0.743	(6)
PDMAPS+LiCl+CNT	60	80	62	1.013	(11)
Carbon sphere+LiCl	60	80	30	0.895	(25)
SiO_2 sphere+LiCl	50	70	21	1.39	(30)
KGM+HPC+LiCl	60	60	15	1.268	(28)
PAM+LiCl+CNT	75	60	229	1.764	(31)
		45	Can't desorb 80% wu		
LiCl@active carbon fibre felt+PTFE membrane	70	80	Can't desorb 80% wu		(32)
PNIPAM-co-DMAPS+LiCl	60	**60**	10	0.806	This work
		40	20	0.834	

S2.13 Chemical composition of water-processable Ppy

As shown in Figure S14a, the Ppy:PSS can be well dispersed in water after long-time standing. Figure S14b presents the FTIR spectra of synthesized Ppy:PSS. The bands located at 1564 and 1449 cm^{-1} are assigned to the characteristic symmetric and asymmetric stretching modes in the pyrrole ring, respectively. The doping state of PPy is indicated by the band at 925 cm^{-1}, which as such confirms the incorporation of dopant ions into the grown polymer. The peak at 1170 cm^{-1} is assigned to the S=O stretching in PSS (33, 34).

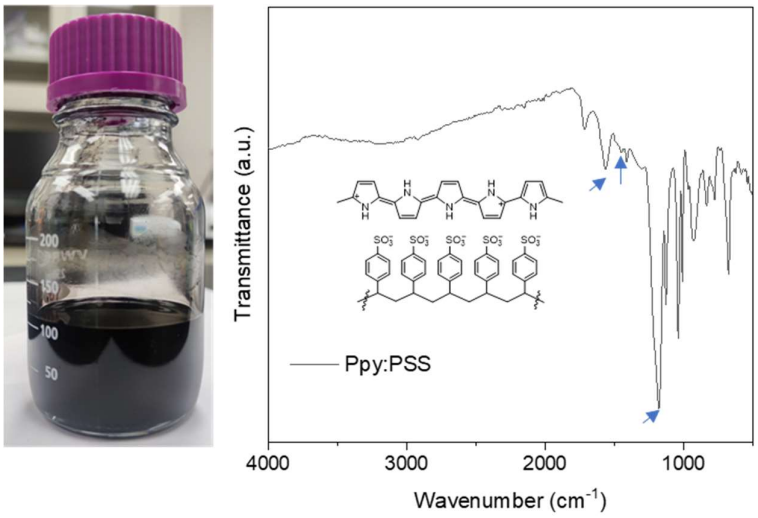

Figure S14. **Ppy:PSS solution and chemical composition** (a) Photograph of Ppy:PSS solution after placing over 1 month. (b) FT-IR spectra and chemical structure of Ppy:PSS.

S2.14 Morphology of water-processable Ppy

As shown in Figure S15, the as-synthesized Ppy:PSS is composed of PSS-wrapped Ppy nanoparticles. The Ppy nanoparticles have sizes of less than 50 nm, and they may form aggregates with a size of around 500 nm. Such a small size combined with the strong hydrophilicity of PSS endows the Ppy:PSS with favorable water processability.

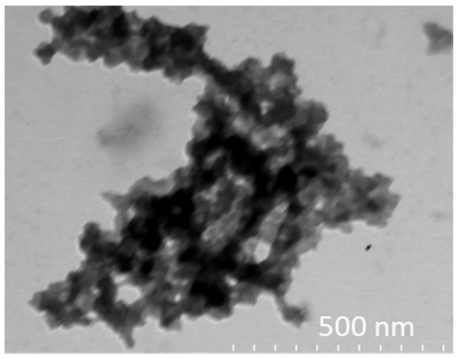

Figure S15. **Morphology of water-processable Ppy**. STEM image of Ppy:PSS.

S2.15 Morphology of water-processable Ppy

As shown in Figure S16, PZMGs all appear as microparticles with diameters of ~50-100 μm. The incorporation content of Ppy:PSS does not affect the microgel morphology.

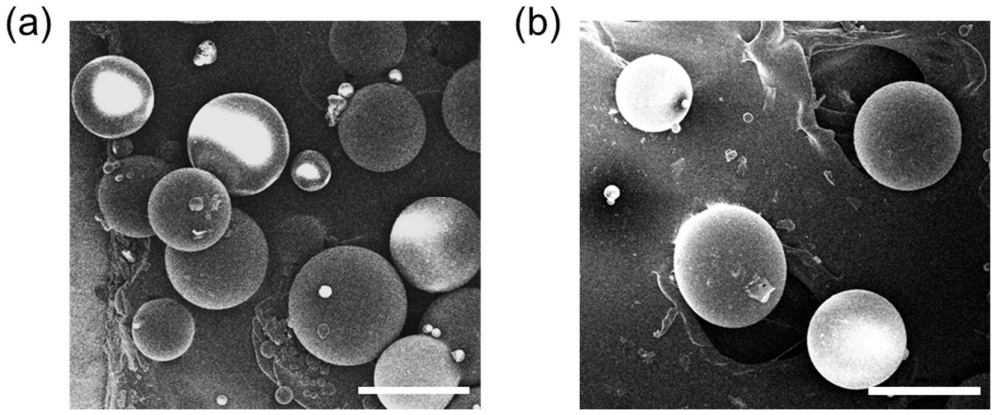

Figure S16. **Morphology of PZMG**. SEM image of (a) PZMG-1 and (b) PZMG-4.

S2.16 Illustration of the photothermal desorption process

In a conventional AWH system, heat will be generated at the solar absorber layer consisting of photothermal materials, and then transferred to the sorbent through a heat transfer layer so that the absorbed water can be released in form of vapor through the evaporation process (Figure S17a). However, due to the existence of thermal resistances, lots of heat will be lost when conducted within the layer as well as at the interface between different layers. Extra thermal energy will also be consumed to raise the temperature of the transfer layer, which further decreases the amount of heat that can be used for water evaporation. Apart from that, the weight of the whole system will be increased with the additives (an extra heat transfer layer, etc.), which will harm the gravimetric capacity of the sorbent (35).

For our system, polypyrrole nanoparticles (Ppy NPs) are well dispersed in the microgel and function as solar absorbers. By converting solar energy into thermal energy, Ppy NP will directly heat its surrounding polymer chains and drive water evaporation (Figure S17b). The heat will be confined near the absorber, and absorbed by the small amount of water in the molecular meshes, thus facilitating water release (36, 37). Besides, heat will also be reinforced between microgels (denoted by the redder area in Figure S17b), which can further enhance the evaporation process. Therefore, benefiting from heat confinement and reinforcement, the absorbed water can be released under relatively low temperatures and weak solar energy input.

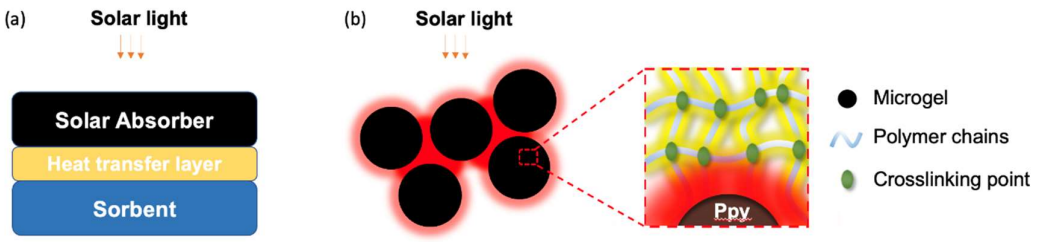

Figure S17. Comparison of the water desorption process in conventional AWH system and our system. (a) Conventional AWH system has a separated solar absorber layer and sorbent layer. (b) Our integrated system with heat confinement and reinforcement.

S2.17 Atmospheric water extraction of PZMG at 30% RH

PZMG can stably operate at 30% RH over 12 cycles in 24 h with an average water uptake of 0.41 g g^{-1}, water release of 0.36 g g^{-1}, and water collection of 0.27 g g^{-1} per cycle. The results validate the feasibility of PZMG work in low RH conditions.

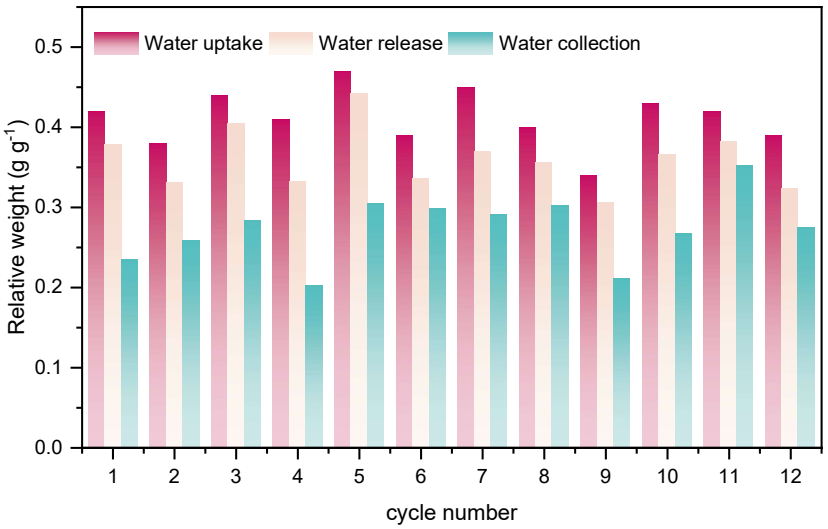

Figure S18. Atmospheric water extraction test. Batch cycling performance at 30% RH sorption environment.

S2.18 The state of salt ions before and after cycling operation

The dynamic behavior of water during the sorption-desorption process within the TZMGs/PZMGs implies potential diffusion of water and resultant ions throughout the polymer network. The thermoresponsive PNIPAM segment undergoes a hydrophilic-to-hydrophobic transition during desorption, which disrupts the hydrogen-bonding water network and facilitates water release. This process could potentially lead to displacement of water molecules carrying salt ions throughout the polymer structure.

To investigate the state and distribution of the salt ions, TGA was employed to evaluate the salt content within the hydrogel samples both before and after the recycling process (Figure S19a). TGA results revealed a consistent salt ion content of ~17.5 wt%, suggesting no significant leakage of salt ions even after 20 cycles. Further structural information about the salt ions within the hydrogel was obtained through XRD studies process (Figure S19b). The absence of salt-related peaks in the XRD patterns post-cycling indicates that the salt ions remain dispersed at the molecular level within the hydrogel, without aggregating into crystalline salt structures.

This information indicates that the salt ions are effectively retained within the hydrogel matrix throughout the sorption-desorption cycles, minimizing leakage and ensuring the enduring efficiency of our TZMGs. These findings support the proposed mechanism for the behavior of our hydrogels during repeated cycles of water absorption and release.

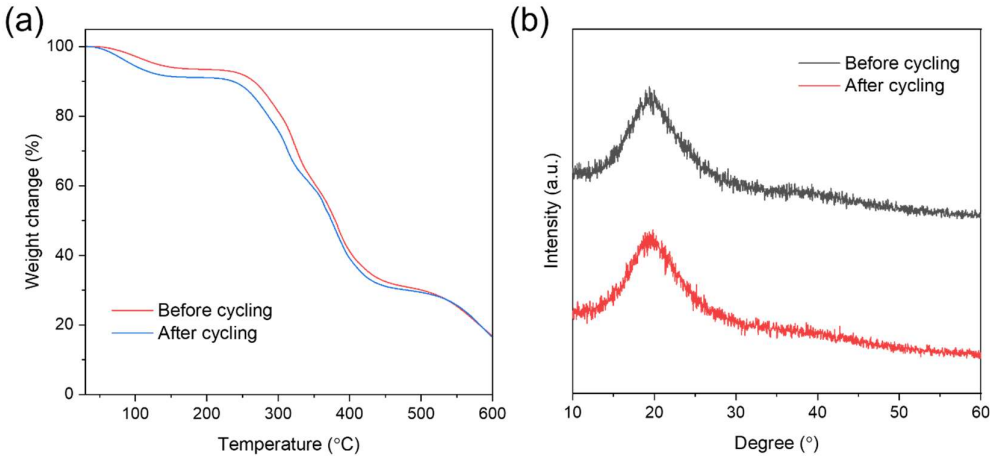

Figure S19. The state of salt ions before and after 20 sorption-desorption cycles. The (a) TGA curves (b) XRD patterns of the hydrogels before and after 20 cycles.

Supplementary reference

1. A. Wexler, S. Hasegawa, Relative humidity-temperature relationships of some saturated salt solutions in the temperature. *Journal of research of the National Bureau of standrds* **53**, 19-26 (1954).
2. B. Sun, Y. Lin, P. Wu, H. W. Siesler, A FTIR and 2D-IR Spectroscopic Study on the Microdynamics Phase Separation Mechanism of the Poly(N-isopropylacrylamide) Aqueous Solution. *Macromolecules* **41**, 1512-1520 (2008).
3. H. G. Schild, Poly(N-isopropylacrylamide): experiment, theory and application. *Prog. Polym. Sci.* **17**, 163-249 (1992).
4. X. Wang *et al.*, An Interfacial Solar Heating Assisted Liquid Sorbent Atmospheric Water Generator. *Angew. Chem. Int. Ed.* **58**, 12054-12058 (2019).
5. C. Peng, L. Chen, M. Tang, A database for deliquescence and efflorescence relative humidities of compounds with atmospheric relevance. *Fundam. Res.* **2**, 578-587 (2022).
6. F. Deng, C. Wang, C. Xiang, R. Wang, Bioinspired topological design of super hygroscopic complex for cost-effective atmospheric water harvesting. *Nano Energy* **90**, 106642 (2021).
7. R. Li, Y. Shi, M. Wu, S. Hong, P. Wang, Photovoltaic panel cooling by atmospheric water sorption–evaporation cycle. *Nat. Sustain.* **3**, 636-643 (2020).
8. H. Lu *et al.*, Tailoring the Desorption Behavior of Hygroscopic Gels for Atmospheric Water Harvesting in Arid Climates. *Adv. Mater.* **34**, 2205344 (2022).
9. J. Xu *et al.*, Efficient Solar-Driven Water Harvesting from Arid Air with Metal–Organic Frameworks Modified by Hygroscopic Salt. *Angew. Chem. Int. Ed.* **59**, 5202-5210 (2020).
10. C. Lei *et al.*, Polyzwitterionic Hydrogels for Efficient Atmospheric Water Harvesting. *Angew. Chem. Int. Ed.* **61**, e202200271 (2022).
11. S. Aleid *et al.*, Salting-in Effect of Zwitterionic Polymer Hydrogel Facilitates Atmospheric Water Harvesting. *ACS Mater. Lett.* **4**, 511-520 (2022).
12. A. Entezari, M. Ejeian, R. Wang, Super Atmospheric Water Harvesting Hydrogel with Alginate Chains Modified with Binary Salts. *ACS Mater. Lett.* **2**, 471-477 (2020).
13. C. D. Díaz-Marín *et al.*, Kinetics of Sorption in Hygroscopic Hydrogels. *Nano Lett.* **22**, 1100-1107 (2022).
14. C. Lei *et al.*, Polyzwitterionic Hydrogels for Highly Efficient High Salinity Solar Desalination. *Angew. Chem. Int. Ed.* **61**, e202208487 (2022).
15. Y. Zhang *et al.*, Effects of Hofmeister Anions on the LCST of PNIPAM as a Function of Molecular Weight. *J. Phys. Chem. C* **111**, 8916-8924 (2007).
16. R. Li *et al.*, Hybrid Hydrogel with High Water Vapor Harvesting Capacity for Deployable Solar-Driven Atmospheric Water Generator. *Environ. Sci. Technol.* **52**, 11367-11377 (2018).
17. G. Yilmaz *et al.*, Autonomous atmospheric water seeping MOF matrix. *Sci. Adv.* **6**, eabc8605 (2020).
18. J. Xu *et al.*, Ultrahigh solar-driven atmospheric water production enabled by scalable rapid-cycling water harvester with vertically aligned nanocomposite sorbent. *Energy Environ. Sci.* **14**, 5979-5994 (2021).
19. F. Deng, C. Xiang, C. Wang, R. Wang, Sorption-tree with scalable hygroscopic adsorbent-leaves for water harvesting. *J. Mater. Chem.* **10**, 6576-6586 (2022).

20. Z. Zhang *et al.*, Sustainable Hierarchical-Pored PAAS–PNIPAAm Hydrogel with Core–Shell Structure Tailored for Highly Efficient Atmospheric Water Harvesting. *ACS Appl. Mater. Interfaces* **14**, 55295-55306 (2022).
21. T. Lyu *et al.*, Macroporous Hydrogel for High-Performance Atmospheric Water Harvesting. *ACS Appl. Mater. Interfaces* **14**, 32433-32443 (2022).
22. H. Yao *et al.*, Highly Efficient Clean Water Production from Contaminated Air with a Wide Humidity Range. *Adv. Mater.* **32**, 1905875 (2020).
23. J. Yang *et al.*, A Moisture-Hungry Copper Complex Harvesting Air Moisture for Potable Water and Autonomous Urban Agriculture. *Adv. Mater.* **32**, 2002936 (2020).
24. W. Yao *et al.*, Loofah Sponge-Derived Hygroscopic Photothermal Absorber for All-Weather Atmospheric Water Harvesting. *ACS Appl. Mater. Interfaces* **14**, 4680-4689 (2022).
25. R. Li, Y. Shi, M. Wu, S. Hong, P. Wang, Improving atmospheric water production yield: Enabling multiple water harvesting cycles with nano sorbent. *Nano Energy* **67**, 104255 (2020).
26. P. A. Kallenberger, M. Fröba, Water harvesting from air with a hygroscopic salt in a hydrogel–derived matrix. *Commun. Chem.* **1**, 28 (2018).
27. W. Guan, C. Lei, Y. Guo, W. Shi, G. Yu, Hygroscopic-Microgels-Enabled Rapid Water Extraction from Arid Air. *Adv. Mater.* **n/a**, 2207786 (2022).
28. Y. Guo *et al.*, Scalable super hygroscopic polymer films for sustainable moisture harvesting in arid environments. *Nat. Commun.* **13**, 2761 (2022).
29. M. Wu *et al.*, Metal- and halide-free, solid-state polymeric water vapor sorbents for efficient water-sorption-driven cooling and atmospheric water harvesting. *Mater. Horizons* **8**, 1518-1527 (2021).
30. K. Yang *et al.*, Hollow spherical SiO2 micro-container encapsulation of LiCl for high-performance simultaneous heat reallocation and seawater desalination. *J. Mater. Chem.* **8**, 1887-1895 (2020).
31. J. Wang *et al.*, High-yield and scalable water harvesting of honeycomb hygroscopic polymer driven by natural sunlight. *Cell Rep. Phys. Sci.* **3**, 100954 (2022).
32. H. Shan *et al.*, High-yield solar-driven atmospheric water harvesting with ultra-high salt content composites encapsulated in porous membrane. *Cell Rep. Phys. Sci.* **2**, 100664 (2021).
33. M. J. González-Tejera, M. A. L. De Plaza, E. D. Sánchez La Blanca, I. Hernández-Fuentes, Electrochemical, FTIR and morphological study of polypyrrole—Polystyrenesulphonate conducting films. *Polym Int.* **31**, 45-50 (1993).
34. T.-M. Wu, H.-L. Chang, Y.-W. Lin, Synthesis and characterization of conductive polypyrrole with improved conductivity and processability. *Polym Int.* **58**, 1065-1070 (2009).
35. Y. Song *et al.*, High-yield solar-driven atmospheric water harvesting of metal–organic-framework-derived nanoporous carbon with fast-diffusion water channels. *Nat. Nanotechnol.* **17**, 857-863 (2022).
36. X. Zhou, F. Zhao, Y. Guo, Y. Zhang, G. Yu, A hydrogel-based antifouling solar evaporator for highly efficient water desalination. *Energy Environ. Sci.* **11**, 1985-1992 (2018).
37. Y. Guo *et al.*, Synergistic Energy Nanoconfinement and Water Activation in Hydrogels for Efficient Solar Water Desalination. *ACS Nano* **13**, 7913-7919 (2019).